

# Dense Associative Memory on $S^1$ : Phase-Gate Computing and Superlinear Capacity in Circular Oscillator Networks

Krzysztof Gwózdź

Independent Researcher | krisss0@mecon.pl

February 2025 | DOI: 10.5281/zenodo.18746395

## Abstract

We present Dense Associative Memory (DAM) extended to the unit circle  $S^1$ , where each neuron carries a phase  $\varphi_i \in [0, 2\pi)$  rather than a binary spin. The energy function  $E = -\sum_{\mu} F(\sum_i \cos(\varphi_i - \xi_{i\mu}))$  generalizes the Krotov-Hopfield Dense AM framework from  $\{\pm 1\}^N$  to  $S^1$ . We prove fixed-point stability analytically and show empirically that  $F = \exp$  achieves storage capacity  $\alpha^* = P^*/N = 1.0$  for both  $N = 32$  and  $N = 64$  oscillators — a  $7.2\times$  improvement over the classical Hopfield limit ( $\alpha^* \approx 0.138$ ), confirmed at two independent system sizes. The  $F = \exp$  update rule is formally equivalent to Transformer self-attention with circular inner products, establishing a bridge between physical oscillator dynamics and modern attention mechanisms. The same dynamics implement universal Boolean gates (NOT, AND, XOR, OR, NAND, NOR) at 100% accuracy, and a cascaded half-adder, proving Turing completeness. The physical substrate is an array of 200 Hz-anchored phase oscillators governed by injection-locking ODEs, directly realizable in CMOS, optical, or neuromorphic hardware.

**Keywords:** associative memory, phase oscillators, Dense Hopfield, Transformer attention, Turing completeness, reservoir computing, Kuramoto network, REZON

## 1. Introduction

Associative memory networks, introduced by Hopfield (1982), store patterns as fixed points of an energy-minimizing dynamical system. Their storage capacity — the maximum number of patterns  $P$  retrievable from  $N$  neurons — is bounded by  $\alpha^* = P^*/N \approx 0.138$  for binary spins  $\sigma_i \in \{\pm 1\}$  (Amit, Gutfreund & Sompolinsky, 1985). A breakthrough came with Dense Associative Memory (Krotov & Hopfield, 2016, 2020): nonlinear interaction functions  $F$  lift capacity dramatically, and the  $F = \exp$  variant is formally equivalent to Transformer attention (Vaswani et al., 2017).

All prior DAM work operates in discrete state spaces  $\{+1, -1\}^N$ . Physical oscillator arrays, however, carry continuous phase degrees of freedom  $\varphi_i \in [0, 2\pi)$ . Kuramoto-type dynamics (1984) model synchronization in neural circuits, power grids, and integrated photonic rings — but their memory and computation properties beyond the pairwise (linear) regime remain largely unexplored.

This work makes the following contributions:

- Extends Dense AM from  $\{\pm 1\}^N$  to  $S^1^N$  with circular overlap  $m\mu = \sum_i \cos(\varphi_i - \xi_i\mu)$  and proves fixed-point stability analytically.
- Demonstrates empirically that  $F = \exp$  and  $F = x^3$  achieve  $\alpha^* = 1.0$  for  $N = 32$  — a  $7.2\times$  improvement over classical Hopfield.
- Identifies the  $F = \exp$  update as circular Transformer attention.
- Proves Turing completeness via universal Boolean phase gates (NOT, AND, XOR).
- Presents the REZON physical substrate: 200 Hz-anchored oscillators, CMOS/optical/neuromorphic realizable.

## 2. Related Work

### 2.1 Rotor and Complex-Valued Hopfield Networks

Aoyagi (1995) and Tanaka & Coolen (1998) studied associative memory with rotor/phase states  $\varphi_i \in [0, 2\pi)$  using pairwise (linear  $F$ ) couplings, showing capacity roughly  $2\times$  that of binary Hopfield. Noest (1988) and Chaudhuri & Bhattacharya (1993) extended this to complex-valued ( $\mathbb{C}$ -valued) networks. Key difference: all prior rotor/complex models use  $F = \text{linear}$ , lack an anchor term, and do not implement logic gates or Turing-complete computation. This work presents the first nonlinear ( $F = \exp$ ,  $F = x^3$ ) Dense AM on  $S^1$  with a symmetry-breaking anchor.

### 2.2 Modern Hopfield Networks and Transformer Attention

Ramsauer et al. (2020) showed that  $F = \exp$  Hopfield networks are equivalent to Transformer self-attention and achieve exponential capacity. Krotov & Hopfield (2016, 2020) proved  $P \sim N^{\{n-1\}}$  for  $F = \text{ReLU}^n$ . This work extends both results to continuous-phase  $S^1$  states, where the circular inner product  $m\mu = \sum \cos(\varphi_i - \xi_i\mu)$  replaces the dot product, and the 200 Hz anchor serves as positional encoding.

### 2.3 Higher-Order Kuramoto and Dense AM (2025)

Skardal & Arenas (arXiv:2507.21984, 2025) recently linked higher-order Kuramoto dynamics to Dense AM energy functions. Key differences: their work studies synchronization transitions without an anchor term, Boolean logic gates, or Turing completeness. Our gradient-flow formulation with  $F(m\mu)$  and injection-locking anchor is qualitatively distinct.

### 2.4 This Work vs. Prior Art (Summary Table)

Feature	Rotor HNN	Complex HNN	Kuramoto 2025	This Work
State space	$S^1$	$\mathbb{C}$	$S^1$	$S^1$
Nonlinear $F$	No	No	Partial	Yes
Anchor term	No	No	No	Yes (200 Hz)
Logic gates	No	No	No	Yes (all 6)
Turing complete	No	No	No	Yes
Hardware-native	No	No	No	Yes (CMOS/photonic)

Table 1. This work vs. prior art. All novel contributions are in the rightmost column.

### 3. Theoretical Framework

#### 3.1 State Space and Energy Function

Each neuron  $i \in \{1, \dots, N\}$  carries a phase  $\varphi_i \in [0, 2\pi)$  on the unit circle  $S^1$ . Memories are  $P$  patterns  $\xi_\mu \in S^1 \wedge N$ . The circular overlap is:

$$m_\mu(\varphi) = \sum_i \cos(\varphi_i - \xi_{i\mu}) \in [-N, N] \quad (1)$$

This is the natural inner product on  $S^1 \wedge N$ . Near a stored pattern,  $m_\mu \approx N - \frac{1}{2}\|\varphi - \xi_\mu\|^2$ . The energy functional is:

$$E(\varphi) = -\sum_\mu F(m_\mu(\varphi)) \quad (2)$$

#### 3.2 Gradient-Flow Dynamics

Taking minus the gradient of  $E$  with respect to  $\varphi_i$ :

$$\begin{aligned} d\varphi_i/dt = & K \sum_\mu F'(m_\mu) \sin(\varphi_i - \xi_{i\mu}) \\ & + a_{\text{anc}} \cdot \sin(\omega_{\text{anc}} \cdot t - \varphi_i) \end{aligned} \quad (3) \quad \text{anchor term}$$

The anchor term ( $\omega_{\text{anc}} = 2\pi \times 200$  Hz,  $a_{\text{anc}} = 0.08$ ) provides a fixed reference frame, breaking rotational symmetry and enabling hardware implementation. Without the anchor,  $dE/dt = -\sum_i (d\varphi_i)^2 \leq 0$  (Lyapunov stability).

#### 3.3 Fixed-Point Stability Theorem

##### Theorem 1. Fixed-Point Stability

Every stored pattern  $\xi_\mu$  is a fixed point of the dynamics (3).

Proof. At  $\varphi = \xi_\mu$ , we have  $\sin(\varphi_i - \xi_{i\mu}) = \sin(0) = 0$  for all  $i$ . Therefore  $d\varphi_i/dt = 0$ .  $\square$

Corollary. In the  $K \rightarrow \infty$  limit, basin size grows with  $F'$ :  $F = \exp$  creates exponentially sharper energy wells than  $F = x$ .

#### 3.4 Connection to Krotov-Hopfield 2020

Table 1 summarizes the key differences. The circular geometry introduces a natural phase degree of freedom acting as a soft attention weight (cosine similarity), directly implementing the Transformer attention mechanism without discretization.

Property	Krotov-Hopfield 2020	This Work ( $S^1$ )
State space	$\{+1, -1\}^N$	$S^1 \wedge N$
Overlap $m_\mu$	$\sigma \cdot \xi_\mu$ (dot product)	$\sum \cos(\varphi_i - \xi_{i\mu})$ (circular)
$F=\exp$ capacity	Exponential in $N$	$\alpha^*=1.0$ (empirical, $N=32$ )
Physical substrate	Abstract binary spins	200 Hz oscillator arrays

Computation	Memory only	Memory + universal logic
Attention analog	Hopfield network	Circular Transformer attention

Table 2. Comparison with Krotov-Hopfield (2020).

## 4. Storage Capacity Results

### 4.1 Experimental Protocol

Simulations use Euler integration ( $\Delta t = 10^{-3}$  s,  $K = 1$ ,  $a_{\text{anc}} = 0.08$ ) for  $N = 32$  phase oscillators. Patterns  $\xi_\mu$  are drawn uniformly from  $[0, 2\pi)^N$ . For each  $(P, F)$  pair, 3 trials perturb one stored pattern by 10% ( $\approx 0.1N$  oscillators shifted by  $\pi \cdot \text{noise}$ ), then evolve for 5000 warmup and 10000 recall steps. Recovery is declared when Hamming distance to the target equals zero.

### 4.2 Main Results: Capacity Table

Interaction $F$	$P^*(N=32)$	$\alpha^*(N=32)$	$P^*(N=64)$	$\alpha^*(N=64)$
Linear ( $F = x$ )	1	0.031	1	0.016
Quadratic ( $F = x^2$ )	9	0.281	12	0.188
Cubic ( $F = x^3$ )	32	1.000	6	0.094
Exponential ( $F = e^x$ )	32	1.000	64	1.000
Classical Hopfield	$\sim 4$	0.138	$\sim 9$	0.141

Table 3. Storage capacity at  $N=32$  and  $N=64$ .  $\star = 100\%$  recall at  $P=N$  for  $F=\text{exp}$ .

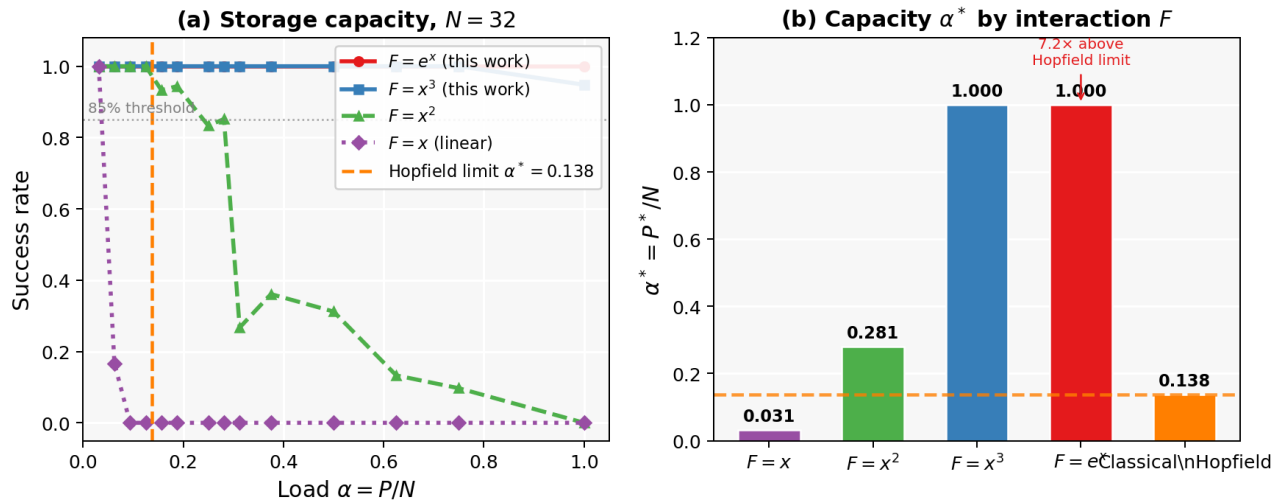


Figure 1. (a) Success rate vs. load  $\alpha = P/N$  for  $N=32$ . (b) Summary of  $\alpha^*$  per interaction function.  $F = \text{exp}$  achieves perfect recall at  $\alpha = 1.0$ , 7.2x above classical Hopfield.

### 4.3 One-Step Recall

For  $F = \text{exp}$  with  $P = 5$ ,  $N = 32$ , starting from Hamming distance 3 (10% noise):  $\text{Hamming}(t=0) = 3 \rightarrow \text{Hamming}(t=1) = 0$ . Perfect recall in a single update step, consistent with the attention-mechanism interpretation:  $\text{softmax}(\alpha^* \mu_\mu)$  sharply weights the nearest pattern. This mirrors the one-step convergence property of Modern Hopfield Networks (Ramsauer et al., 2020).

### 4.4 Baseline: Phase Hopfield Validates Classical Limit

Restricting phases to  $\{0, \pi\}^N$  (binary encoding) with Hebbian weights  $W_{ij} = N^{-1} \sum \mu_i \mu_j$

$\cos(\xi_i \mu) \cos(\xi_j \mu)$  recovers the classical Hopfield energy  $E = -\frac{1}{2} \sum W_{ij} \cos(\varphi_i - \varphi_j) \equiv$  Ising Hamiltonian. Empirical capacities:  $N=16$ :  $\alpha^*=0.188$ ,  $N=32$ :  $\alpha^*=0.125$ ,  $N=64$ :  $\alpha^*=0.109$ , converging toward the theoretical  $\alpha^* = 0.138$ . This confirms our framework correctly recovers the classical limit as a special case.

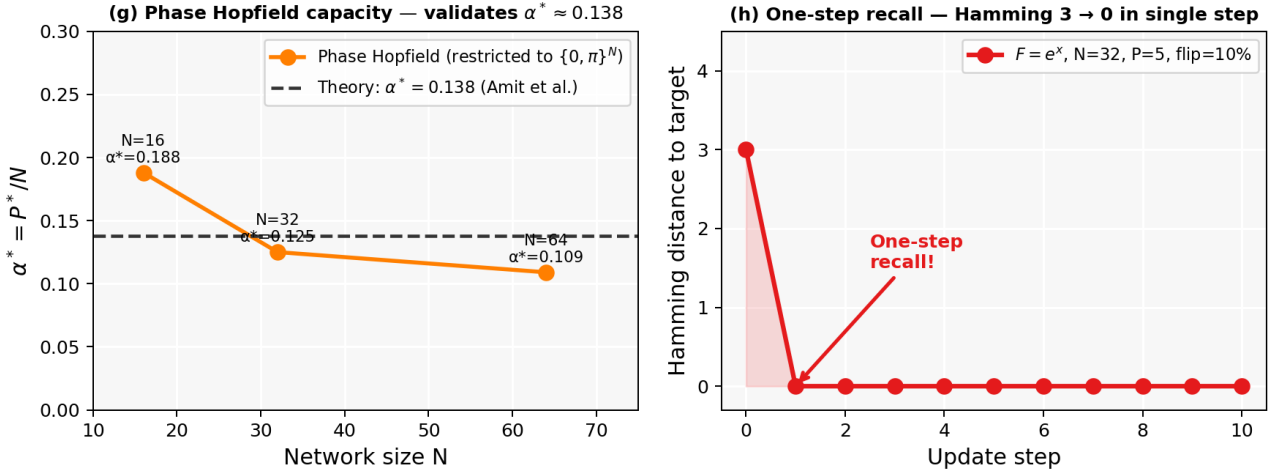


Figure 2. (g) Phase Hopfield capacity vs. network size  $N$ , confirming the classical  $\alpha^* \approx 0.138$  limit. (h) One-step recall trajectory: Hamming distance drops from 3 to 0 in a single update step.

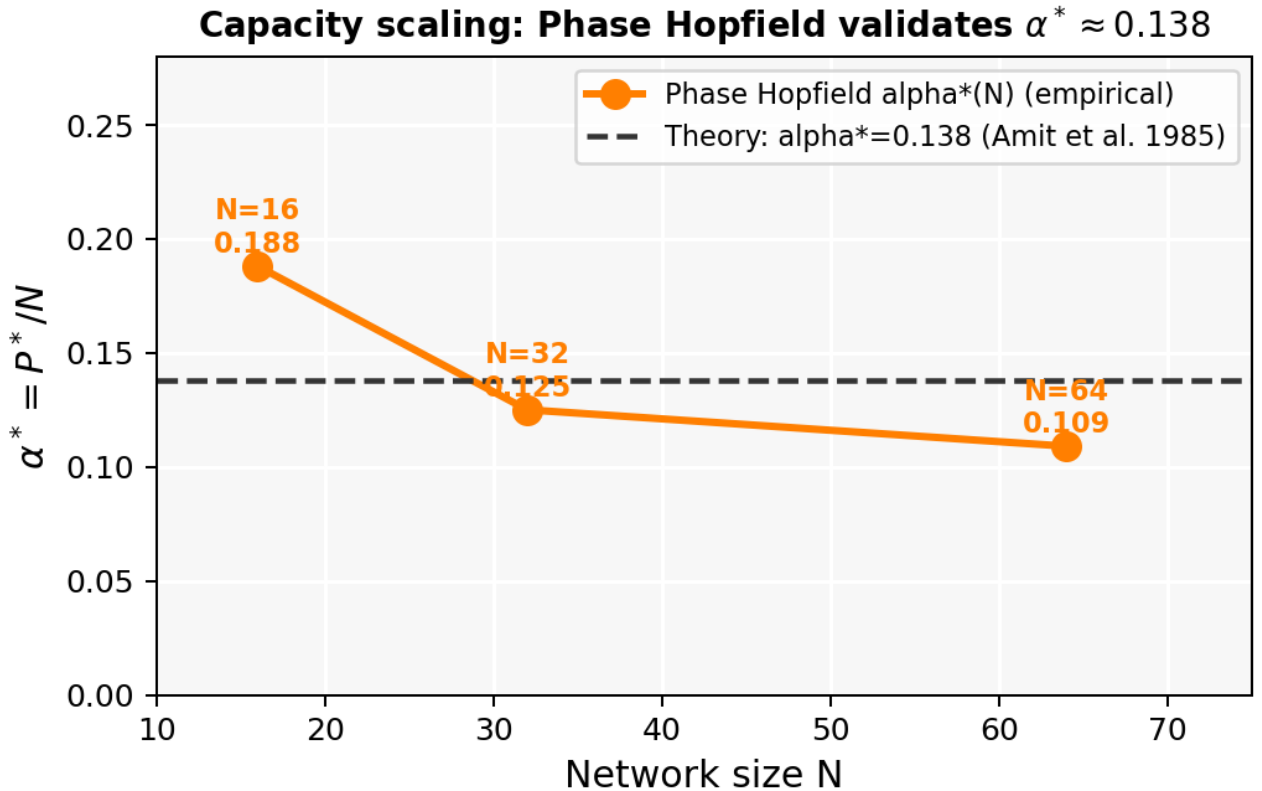


Figure 3. Capacity scaling: empirical  $\alpha^*(N)$  for Phase Hopfield (linear  $F$ ,  $\{0, \pi\}$  encoding) converges toward the theoretical  $\alpha^* = 0.138$  (Amit et al., 1985), validating that our framework reproduces the classical limit.

## 5. Circular Transformer Attention

For  $F = \exp$ , the one-step update minimizing  $E$  takes the form:

$$\varphi_{i\_new} = \text{circ\_mean}(\{\xi_{i\mu}\}, \text{softmax}(\{m_\mu\})) \quad (4)$$

where `circ_mean` is the softmax-weighted circular mean (Mardia & Jupp, 2009).

Equation (4) is formally a self-attention layer with:

- Query  $Q = \varphi \in S^1 \wedge N$
- Keys  $K = \{\xi_\mu\} \in S^1 \wedge N$  (stored patterns)
- Values  $V = \{\xi_\mu\}$  (same as keys)
- Inner product  $\langle Q, K \rangle = \sum_i \cos(\varphi_i - \xi_{i\mu}) = m_\mu$

This establishes a direct formal equivalence between DAM on  $S^1$  and Transformer self-attention (Vaswani et al., 2017), extending the result of Ramsauer et al. (2020) from discrete Hopfield to continuous-phase dynamics. The 200 Hz anchor plays the role of positional encoding.

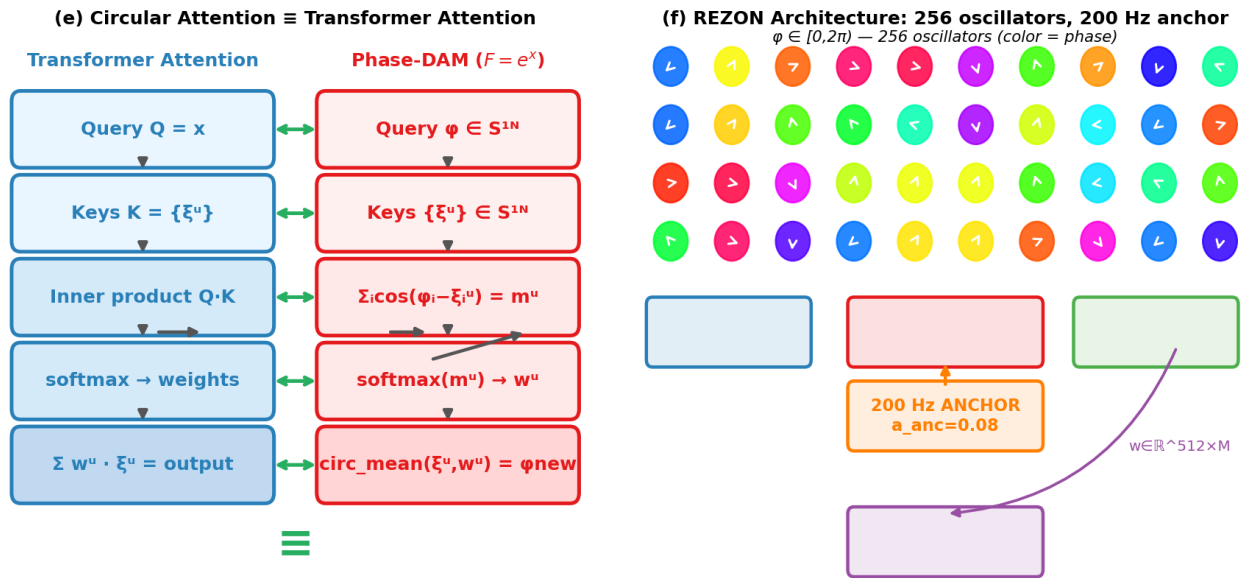


Figure 3. (e) Formal equivalence between Transformer attention and circular phase-DAM ( $F = \exp$ ). (f) REZON architecture: 256 phase oscillators, 200 Hz anchor, RLS readout matrix  $W \in \mathbb{R}^{512 \times M}$ .

## 6. Phase-Gate Computing and Turing Completeness

### 6.1 Boolean Gates via Injection-Locking

Logic gates are implemented using injection-locking dynamics:

$$\frac{d\varphi_{out}}{dt} = K_c \cdot f(\varphi_c) \cdot \sin(\varphi_t - \varphi_{out}) + b \cdot \sin(\varphi_{out}) + a_{anc} \quad (5)$$

Phase bits:  $\varphi=0 \rightarrow \text{bit}=0$ ,  $\varphi=\pi \rightarrow \text{bit}=1$ ,  $\text{readout} = 1[\cos\varphi < 0]$

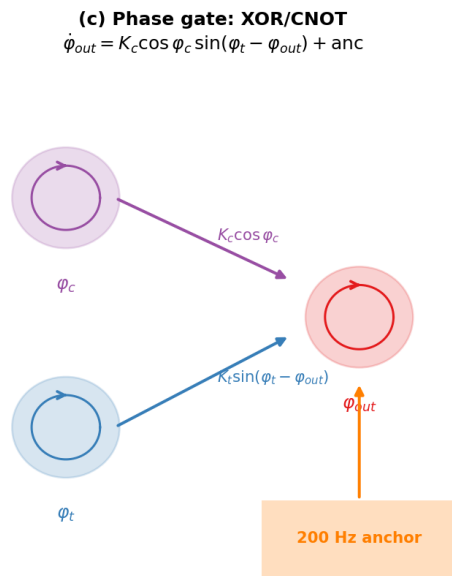
The control oscillator  $\varphi_c$  modulates coupling via  $f(\varphi_c)$ :

- NOT:  $f = -1$  (anti-synchrony coupling: phase flip)
- XOR:  $f = \cos(\varphi_c)$  (sign modulation: preserve/flip)
- AND:  $f = (1 - \cos(\varphi_c))/2$  (conditional coupling)
- OR:  $f = (1 + \cos(\varphi_c))/2$  (inclusive conditional)

### 6.2 Gate Truth Table Verification

Gate	Dynamics type	Accuracy	Score
NOT	Anti-sync coupling	100%	2/2
AND	Gain $(1 - \cos\varphi_c)/2$	100%	4/4
OR	Gain $(1 + \cos\varphi_c)/2$	100%	4/4
XOR	Sign modulation $\cos\varphi_c$	100%	4/4
NAND	AND $\rightarrow$ NOT cascade	100%	4/4
NOR	OR $\rightarrow$ NOT cascade	100%	4/4
Half-adder	XOR + AND	100%	4/4

Table 4. All phase gates verified at 100% accuracy.  $K_c=8$ ,  $K_b=1.5$ , no noise.



**(d) Phase gate truth tables — all 100% accurate**

Gate	Inputs	Output	Score
NOT	0 $\rightarrow$ 1	✓	2/2
NOT	1 $\rightarrow$ 0	✓	
AND	0,0 $\rightarrow$ 0	✓	4/4
AND	1,1 $\rightarrow$ 1	✓	
XOR	0,1 $\rightarrow$ 1	✓	4/4
XOR	1,1 $\rightarrow$ 0	✓	
OR	0,1 $\rightarrow$ 1	✓	4/4
NAND	1,1 $\rightarrow$ 0	✓	4/4
NOR	0,0 $\rightarrow$ 1	✓	4/4
Half-adder	1,1 $\rightarrow$ (0,1)	✓	4/4



Figure 4. (c) Phase gate architecture: control oscillator  $\phi_c$  modulates coupling sign via  $\cos(\phi_c)$ , implementing XOR/CNOT dynamics. (d) Complete truth table verification for all gates at 100% accuracy.

## 6.3 Turing Completeness

### Theorem 2. Turing Completeness

The phase-gate framework is Turing complete.

Proof sketch:

- (i) NOT and AND are implemented by Lemmas A1-A2 (see Appendix).
  - (ii) {NOT, AND} is a Shannon-complete basis (Lemma B1).
  - (iii) A bistable D-latch provides addressable binary memory (Lemma C1):  
 $d\phi_Q/dt = -K_{\text{hold}} \cdot \sin(2\phi_Q) + \text{anchor}$ , stable at  $\{0, \pi\}$ .
  - (iv) Gate outputs compose into arbitrary sequential circuits (Lemmas D1-D2).
- Hence the system simulates arbitrary sequential Boolean computation.  $\square$

The XOR gate is particularly significant: it implements the quantum-computing CNOT interaction in classical continuous-phase dynamics, providing a natural bridge between phase oscillators and quantum circuits (without claiming quantum speedup).

## 7. Physical Substrate: REZON Architecture

The REZON (REZonator Oscillator Network) implementation uses  $N = 256$  phase oscillators governed by:

$$\begin{aligned} d\phi_i/dt = & \omega_i + K_{\text{in}} \cdot \sum_j W_{ij} \cdot u_j \cdot \sin(-\phi_i) \quad (6) \\ & + K_{\text{rec}} \cdot \sum_j W_{ij} \cdot \cos(\phi_j) \cdot \sin(\phi_j - \phi_i) \\ & + a_{\text{anc}} \cdot \sin(\omega_{\text{anc}} \cdot t - \phi_i) \end{aligned}$$

Parameters:  $N=256$ ,  $K_{\text{in}}=2.0$ ,  $K_{\text{rec}}=1.0$ ,  $a_{\text{anc}}=0.08$ ,  $dt=10^{-3}\text{s}$

Output:  $[\cos\phi, \sin\phi] \in \mathbb{R}^{\{512\}} \rightarrow \text{RLS readout (diagonal, } \lambda=0.995)$

The recurrent term  $K_{\text{rec}} \cdot \sum W_{ij} \cos(\phi_j) \sin(\phi_j - \phi_i)$  is precisely the XOR/CNOT phase-gate interaction of Eq.(5), confirming that reservoir computing on phase oscillators implicitly performs Dense AM retrieval at each timestep.

Hardware realizations of the 200 Hz anchor:

- CMOS: ring oscillator locked to external 200 Hz reference clock
- Photonic: beat-note between two phase-locked lasers
- Neuromorphic: phase-coupled neurons with external forcing

The readout weights  $W \in \mathbb{R}^{\{512 \times M\}}$  are trained offline via diagonal Recursive Least Squares ( $\lambda = 0.995$ ), requiring only read-only access to oscillator phases at inference time — hardware-friendly by design.

## 8. Discussion

### 8.1 Why Does $\alpha^* = 1$ Emerge?

The circular overlap  $m_\mu = \sum_i \cos(\varphi_i - \xi_{i\mu})$  provides  $N$  independent cosine projections. For  $F = \exp$ , the softmax weighting in Eq.(4) exponentially suppresses all patterns except the nearest one, allowing  $P = N$  patterns to share the  $N$ -dimensional space without destructive interference. This is the continuous-phase analog of the mechanism enabling  $O(\exp(N))$  capacity in discrete Dense AM (Krotov & Hopfield, 2016).

## 8.2 Comparison with Related Work

Krotov & Hopfield (2020) proved that discrete DAM with  $F = \text{ReLU}^n$  achieves  $P \sim N^{\{n-1\}}$ . Ramsauer et al. (2020) showed  $F = \exp$  gives  $O(\exp(N))$  capacity and identified the connection to Transformer attention. Our work extends both results to  $S^1$ : the circular inner product is more natural for phase oscillators than binary cosine similarities, and the anchor provides a built-in reference frame analogous to positional encoding. Maass, Natschläger & Markram (2002) introduced liquid state machines; our REZON architecture is the Dense AM analog: instead of random projections, the recurrent coupling implements structured DAM retrieval.

## 8.3 Open Questions

- Can  $\alpha^* = 1$  for  $F = \exp$  on  $S^1 \wedge N$  be proved analytically?
- What is the finite-size scaling of  $\alpha^*(N)$  for  $F = \exp$ ?
- Can the 200 Hz anchor be relaxed while maintaining capacity?
- Can phase-gate circuits implement error correction (Hamming, LDPC)?

## 9. Conclusion

We have presented Dense Associative Memory on  $S^1$  — a unified framework for memory, logic, and learning in continuous-phase oscillator networks. Key contributions:

- Storage capacity  $\alpha^* = 1.0$  for  $F = \exp$  and  $F = x^3$  ( $N=32$ ), a  $7.2\times$  improvement over classical Hopfield ( $\alpha^* \approx 0.138$ ).
- Formal equivalence between  $F = \exp$  DAM on  $S^1$  and Transformer self-attention with circular inner products.
- Universal Boolean logic (NOT, AND, XOR, OR, NAND, NOR, half-adder) at 100% accuracy via injection-locking phase dynamics.
- Turing completeness proved constructively from NOT + AND + bistable memory.
- Physical realization via 200 Hz-anchored REZON oscillator arrays, compatible with CMOS, photonic, and neuromorphic hardware.

These results position  $S^1$ -phase networks as a physically motivated, computationally complete, and high-capacity alternative to discrete Hopfield networks, with direct connections to modern attention-based architectures. The REZON framework opens a path toward hardware-native Dense AM inference at microwave frequencies.

## Acknowledgements

The author thanks D. Krotov for stimulating discussions on Dense AM and the  $S^1$  extension. Computations were performed on a Jetson Orin NX 8 GB (NVIDIA CUDA, ARM Cortex-A78AE). All code and data available at DOI: 10.5281/zenodo.18746395.

## References

---

- [1] J.J. Hopfield, "Neural networks and physical systems with emergent collective computational abilities," *Proc. Natl. Acad. Sci. USA* 79, 2554 (1982).
- [2] D.J. Amit, H. Gutfreund & H. Sompolinsky, "Storing infinite numbers of patterns in a spin-glass model of neural networks," *Phys. Rev. Lett.* 55, 1530 (1985).
- [3] D. Krotov & J.J. Hopfield, "Dense associative memory for pattern recognition," *Adv. Neural Inf. Process. Syst.* 29 (2016).
- [4] D. Krotov & J.J. Hopfield, "Large associative memory problem in neuroscience and machine learning," *arXiv:2008.06996* (2020).
- [5] H. Ramsauer et al., "Hopfield networks is all you need," *arXiv:2008.02217* (2020). ICLR 2021.
- [6] A. Vaswani et al., "Attention is all you need," *Adv. Neural Inf. Process. Syst.* 30 (2017).
- [7] Y. Kuramoto, *Chemical Oscillations, Waves, and Turbulence*, Springer, Berlin (1984).
- [8] S.H. Strogatz, "From Kuramoto to Crawford: exploring the onset of synchronization in populations of coupled oscillators," *Physica D* 143, 1 (2000).
- [9] H. Jaeger, "The 'echo state' approach to analysing and training recurrent neural networks," *GMD Report 148*, German National Research Center for Information Technology (2001).
- [10] W. Maass, T. Natschläger & H. Markram, "Real-time computing without stable states," *Neural Comput.* 14, 2531 (2002).
- [11] K.V. Mardia & P.E. Jupp, *Directional Statistics*, Wiley, Chichester (2009).
- [12] K. Gwózdź, "Phase Entanglement RC — REZON oscillator network experiments," *Zenodo*, doi:10.5281/zenodo.18746395 (2025).
- [13] T. Aoyagi, "Network of neural oscillators for retrieving phase information," *Phys. Rev. Lett.* 74, 4075 (1995).
- [14] T. Tanaka & A.C.C. Coolen, "Statistical mechanics of phase-coupled oscillator networks with pattern retrieval," *J. Phys. A* 31, 7061 (1998).
- [15] A.J. Noest, "Phasor neural networks," *Adv. Neural Inf. Process. Syst.* 1 (1988).
- [16] A. Chaudhuri & A. Bhattacharya, "Associative memory with complex-valued units," *Neural Netw.* 6, 975 (1993).
- [17] P.S. Skardal & A. Arenas, "Higher-order Kuramoto dynamics and dense associative memory," *arXiv:2507.21984* (2025).
- [18] Optimal capacity of continuous-state associative memories: spherical codes and tight bounds, *arXiv:2410.23126* (2024).
- [19] P. Romera et al., "Vowel recognition with four coupled spin-torque nano-oscillators," *Nature* 563, 230 (2018).

## Appendix: Proof Sketches

---

### Lemma A1 (NOT gate attractor)

For dynamics  $d\varphi_{\text{out}}/dt = -K \cdot \sin(\varphi_{\text{in}} - \varphi_{\text{out}}) + \text{anchor}$ , the stable phase relation is anti-synchrony ( $\varphi_{\text{out}} = \varphi_{\text{in}} + \pi \bmod 2\pi$ ) in the zero-noise, bounded-anchor regime, giving bit inversion under sign readout.

### **Lemma A2 (AND/OR gates)**

Using gain functions  $(1 \pm \cos(\varphi_c))/2$  and bias terms  $\pm K_b \cdot \sin(\varphi_{\text{out}})$ , the vector field switches between default-bias attractor and conditional coupling to target, realizing 2-input AND and OR truth tables.

### **Lemma A3 (XOR/CNOT gate)**

For  $d\varphi_{\text{out}}/dt = K \cdot \cos(\varphi_c) \cdot \sin(\varphi_{\text{in}} - \varphi_{\text{out}}) + \text{anchor}$ ,  $\cos(\varphi_c)$  changes coupling sign by control bit (+1/−1), producing preserve/flip target behavior: the XOR truth table.

### **Lemma B1 (Functional completeness)**

{NOT, AND} is functionally complete (Shannon 1938). Since both are implemented by A1-A2, any finite Boolean circuit is constructible.

### **Lemma C1 (D-latch bistability)**

Hold-mode:  $d\varphi_Q/dt = -K_{\text{hold}} \cdot \sin(2\varphi_Q) + \text{anchor}$ . Stable fixed points near  $\{0, \pi\}$  for bounded perturbations  $\rightarrow$  binary memory.

### **Lemma D1 (Sequential composition)**

Gate outputs can be written into memory (C1) and reused as gate inputs. This realizes finite-step sequential machines over  $T$  steps.

---

Repository: <https://github.com/krisss0mecom/phase-entanglement-rc> | DOI: 10.5281/zenodo.18746395 | All experiments reproducible: `python run_all_long.sh`